Universal architecture of bacterial chemoreceptor arrays

Ariane Briegel[a,b], Davi R. Ortega[c,d], Elitza I. Tocheva[a], Kristin Wuichet[d], Zhuo Li[a,b], Songye Chen[a], Axel Müller[e], Cristina V. Iancu[a,1], Gavin E. Murphy[a,2], Megan J. Dobro[a], Igor B. Zhulin[d,f], and Grant J. Jensen[a,b,3]

Divisions of [a]Biology and [e]Chemistry and [b]Howard Hughes Medical Institute, California Institute of Technology, Pasadena, CA 91125; Departments of [c]Physics and [d]Microbiology, University of Tennessee, Knoxville, TN 37996; and [f]BioEnergy Center and Computer Science and Mathematics Division, Oak Ridge National Laboratory, Oak Ridge, TN 37831

Edited by Laura L. Kiessling, University of Wisconsin, Madison, WI, and approved July 20, 2009 (received for review May 11, 2009)

Chemoreceptors are key components of the high-performance signal transduction system that controls bacterial chemotaxis. Chemoreceptors are typically localized in a cluster at the cell pole, where interactions among the receptors in the cluster are thought to contribute to the high sensitivity, wide dynamic range, and precise adaptation of the signaling system. Previous structural and genomic studies have produced conflicting models, however, for the arrangement of the chemoreceptors in the clusters. Using whole-cell electron cryo-tomography, here we show that chemoreceptors of different classes and in many different species representing several major bacterial phyla are all arranged into a highly conserved, 12-nm hexagonal array consistent with the proposed ''trimer of dimers'' organization. The various observed lengths of the receptors confirm current models for the methylation, flexible bundle, signaling, and linker sub-domains in vivo. Our results suggest that the basic mechanism and function of receptor clustering is universal among bacterial species and was thus conserved during evolution.

bacterial ultrastructure | chemotaxis | electron cryo-tomography

Most motile prokaryotes rely on a chemosensory system to control their movement toward favorable environmental conditions (1). This process of chemotaxis depends on transmembrane chemoreceptors called methyl-accepting chemotaxis proteins (MCPs). MCPs can be classified by topology type (2) and signaling domain class (3). Topology type I MCPs have large periplasmic ligand-binding domains (2) and an elongated cytoplasmic region consisting of a HAMP domain (i.e., histidine kinases, adenylyl cyclases, methyl-binding proteins, and phosphatases) followed by a signaling domain, which in turn is composed of "methylation," "flexible bundle," and "signaling" sub-domains (3, 4) [supporting information (SI) Fig. S1*A*]. MCPs cluster together with other chemotaxis proteins including CheA and CheW in large arrays at the cell pole (5–9).

Because MCPs act cooperatively, their arrangement and interactions within the arrays are critical to their function. Based on the crystal structure of the Tsr receptor from *Escherichia coli* (10), as well as cross-linking and other studies (11, 12), it seems clear now that the basic functional unit in that organism is a "trimer of receptor dimers." It was further proposed that, in *E. coli*, trimers of receptor dimers form a hexagonal array with a lattice spacing of 20 nm (13). A subsequent electron cryo-tomography (ECT) study showed that overexpressed Tsr chemoreceptors in *E. coli* pack into a hexagonal lattice with a center-to-center spacing of 7.5 nm (14–17). In these overexpression strains, the receptors surprisingly form a "zipper-like" double layer, in which large invaginations of the inner membrane allow the cytoplasmic tips of one layer to interact with the cytoplasmic tips of a second, facing layer. This arrangement was at one point proposed to represent the activated form of the receptors (18), but its physiologic relevance was later refuted (19). Adding further complication, MCPs from *Thermotoga maritima* crystalized as rows of dimers (20). This structure, combined with pulsed ESR and crystallographic studies of a CheA-CheW dimer, led to a third "hedgerows of dimers" model for the architecture of chemoreceptor arrays (20). Finally, through direct imaging of intact *Caulobacter crescentus* cells, we (21) and others (22) showed that the chemoreceptors in that organism are arranged in a hexagonal lattice whose 12-nm spacing suggested that trimers of receptor dimers occupied each threefold symmetric vertex. Whereas the MCPs of *E. coli* and 16 of the 18 MCPs of *C. crescentus* belong to the same signaling domain class (36H), those from *T. maritima* belong to a different class (44H) (3). Moreover, certain residues that were seen to make important contacts in the *E. coli* Tsr trimer-of-dimers structure are not conserved in all MCPs. Phenylalanine 373, for example, is involved in hydrophobic trimerization interactions in the Tsr crystal structure, but is replaced by glutamate in all the *T. maritima* chemoreceptors (3, 10, 20). Thus, based on structural and bioinformatics data, it was unclear whether receptors from different MCP classes and organisms clustered similarly, or if not, how many architectures there might be. By imaging WT cells in near-native states, here we show that the chemoreceptors of diverse species from 6 different signaling domain classes are all arranged into a highly conserved, 12-nm hexagonal array consistent with a single "trimer of receptor dimers" functional unit at each vertex.

Results and Discussion

Position of Chemoreceptor Arrays Within Cells. To visualize the arrangement of chemoreceptors in diverse bacteria, we selected 13 distantly related organisms, which together possess receptors from all 7 major signaling domain classes (3) (Table 1) and recorded nearly 700 ECTs of intact, frozen-hydrated cells. Previous immunolabeling (19) and correlated light and EM studies (21) had already established that, in *E. coli* and *C. crescentus*, chemoreceptor arrays can be recognized as clusters of thin, pillar-like densities extending from the inner membrane to a prominent "base plate" formed by CheA and CheW 20 to 30 nm below. Similar structures were seen in all 13 organisms imaged here (Figs. 1 and 2), but their locations within the cell varied. As in *E. coli*, the chemoreceptor arrays in *Magnetospirillum magneticum, Rhodobacter sphaeroides, Treponema primitia, T. maritima*, and *Listeria monocytogenes* were polar. In contrast, the arrays in *Helicobacter hepaticus* and *Campylobacter*

Author contributions: A.B. and G.J.J. designed research; A.B., D.R.O., E.I.T., K.W., Z.L., S.C., A.M., C.V.I., G.E.M., and M.J.D. performed research; A.B., D.R.O., E.I.T., K.W., and I.B.Z. analyzed data; and A.B., D.R.O., E.I.T., I.B.Z., and G.J.J. wrote the paper.

The authors declare no conflict of interest.

This article is a PNAS Direct Submission.

[1]Present address: Department of Biochemistry and Molecular Biology, Rosalind Franklin University, The Chicago Medical School, North Chicago, IL 60064.

[2]Present address: Laboratory of Cell Biology, Center for Cancer Research, National Cancer Institute, National Institutes of Health, Bethesda, MD 20892.

[3]To whom correspondence should be addressed. E-mail: jensen@caltech.edu.

This article contains supporting information online at www.pnas.org/cgi/content/full/0905181106/DCSupplemental.

Table 1. Summary of measurements of 13 different bacterial species obtained by ECT

Bacterium	Phylum	Average cell diameter × length (μm)	MCP class (no. of receptors)[a]	Location	Distance from IM to base plate (nm)	Lattice (nm)	Surface area (nm²), estimated no. of receptors[b]
Thermotoga maritima	Thermotogae	0.5–1 × >1.5	44H (**6**) Unc (1)	Polar	25	12	≈97 k, ≈9,400
Listeria monocytogenes	Firmicutes	0.5 × >1.5	44H (**1**), 24H (1)	Polar	26	None observed	≈30 k, ≈2,900
Acetonema longum	Firmicutes	0.3 × variable length (>10)	44H (**20**,2), Unc (10)	Subpolar	26	12	≈51 k, ≈5,000
Borrelia burgdorferi	Spirochaetes	0.2 × variable length (>10)	34H (**2**), 48H (**1**), Unc (3)	Subpolar	27	None observed	NA
Treponema primitia	Spirochaetes	0.4 × 3–8	48H (**10**,1), 40H (**1**) Unc (**1**,2)	Polar	28	12	≈15 k, ≈1,500
Caulobacter crescentus	Alpha-proteobacteria	0.4–0.7 × 0.9–2.2	36H (**9**,7), 38H (**1**), Unc (1)	Polar, convex side (21)	31	12	≈17 k, ≈1,700
Magnetospirillum magneticum	Alpha-proteobacteria	0.5 × 2–10	38H (**39**,23), 40H (**2**), 44H (1), Unc (7)	Polar	28	12	≈12 k, ≈1,200
Rhodobacter sphaeroides	Alpha-proteobacteria	0.7–0.8 × 1.3–1.4	34H (**7**,1), 36H (2), Unc (2)	Polar	21	12	≈22 k, ≈2,200
Escherichia coli	Gamma-proteobacteria	0.5–1.3 × 2–5	36H (**4**,1)	Mainly polar (19)	22	12	≈53 k, ≈5,200
Vibrio cholera	Gamma-proteobacteria	0.8–0.9 × > 1.5	40H (**32**,10), 44H (1), 36H (2), 24H (2), Unc (2)	Polar, convex side	25	12	≈121 k, ≈11,800
Halothiobacillus neapolitanus	Gamma-proteobacteria	0.4–0.5 × 1.6–1.7	40H (**4**)	Polar	24	12	≈31 k, ≈3,000
Helicobacter hepaticus	Epsilon-proteobacteria	0.3 × 1.5–4	28H (**4**,1) 40H (**3**) Unc (1)	Polar ″cap″	24	12	≈112 k, ≈10,900
Campylobacter jejuni	Epsilon-proteobacteria	0.4 × 0.5–5	28H (**4**), 40H (**1**,1), 24H (3), Unc (1)	Polar ″cap″	24	12	≈144 k, ≈14,400

[a], The receptors present in each genome are listed by organism. The number of receptors in each signaling domain class is listed in column 4 (*Unc*, uncharacterized). After each class, the number of MCPs that do (bold) and do not (regular print) belong to topology class I appear in parenthesis.
[b], Number of receptors per array (last column) estimated from the observed (average) surface areas assuming hexagonally packed receptor trimers of dimers (21).

jejuni formed a polar "collar" completely surrounding the tip of the cell, but with a gap at the apex occupied by the flagellar motor. As in *C. crescentus* (21), the arrays in *Vibrio cholerae* were polar but consistently localized to the convex side of the crescent-shaped cells. Receptor arrays in *Acetonema longum* and *Borrelia burgdorferi* were typically subpolar but inconsistently positioned. The array in *A. longum* was found, for instance, to range from immediately adjacent to the pole to nearly 1 μm away. Although

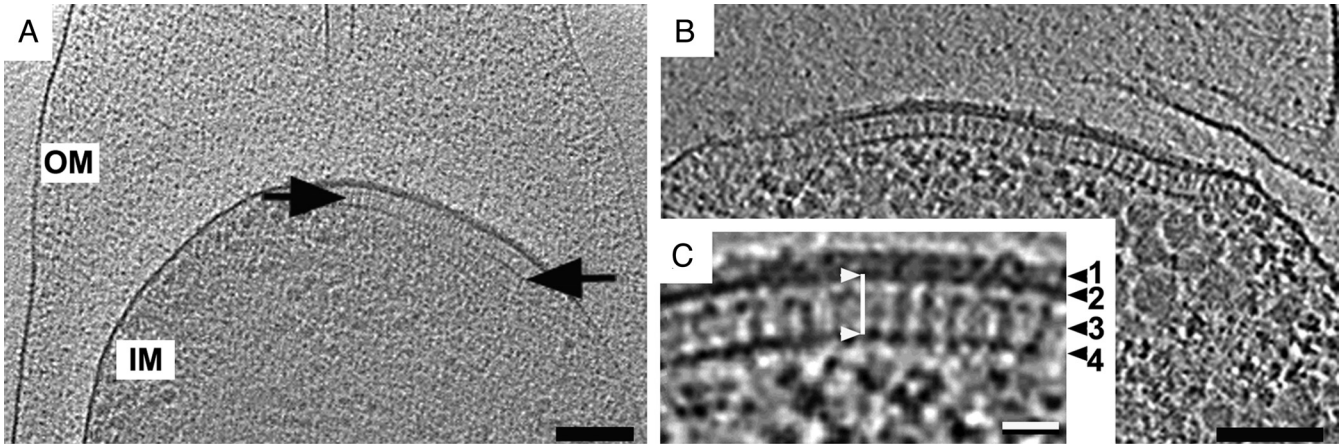

Fig. 1. Characteristic appearance of chemoreceptor arrays in vivo. (*A*) A 55-nm-thick tomographic slice through a *T. maritima* cell pole (signaling domain class 44H). Typical features like the inner membrane (*IM*) and outer membrane (*OM*) and the enclosed extended periplasm are clearly visible. The arrows indicate the location of the chemoreceptor array within the inner membrane and densely packed cytoplasm. (Scale bar: 100 nm.) (*B*) A 3-nm-thick tomographic slice through the pole of a *T. maritima* cell treated with polymyxin B. The reduced cytoplasmic crowding clarifies chemoreceptor features compared with those in untreated cells. (Scale bar: 100 nm.) (*C*) Enlarged view of the array shown in *B*: *1*, periplasmic receptor domains; *2*, inner membrane; *3*, cytoplasmic receptor domains; *4*, CheA-CheW base plate. The line between the white arrows illustrates how the array heights were measured (from the center of the inner membrane to the center of the CheA-CheW base layer). (Scale bar: 25 nm.)

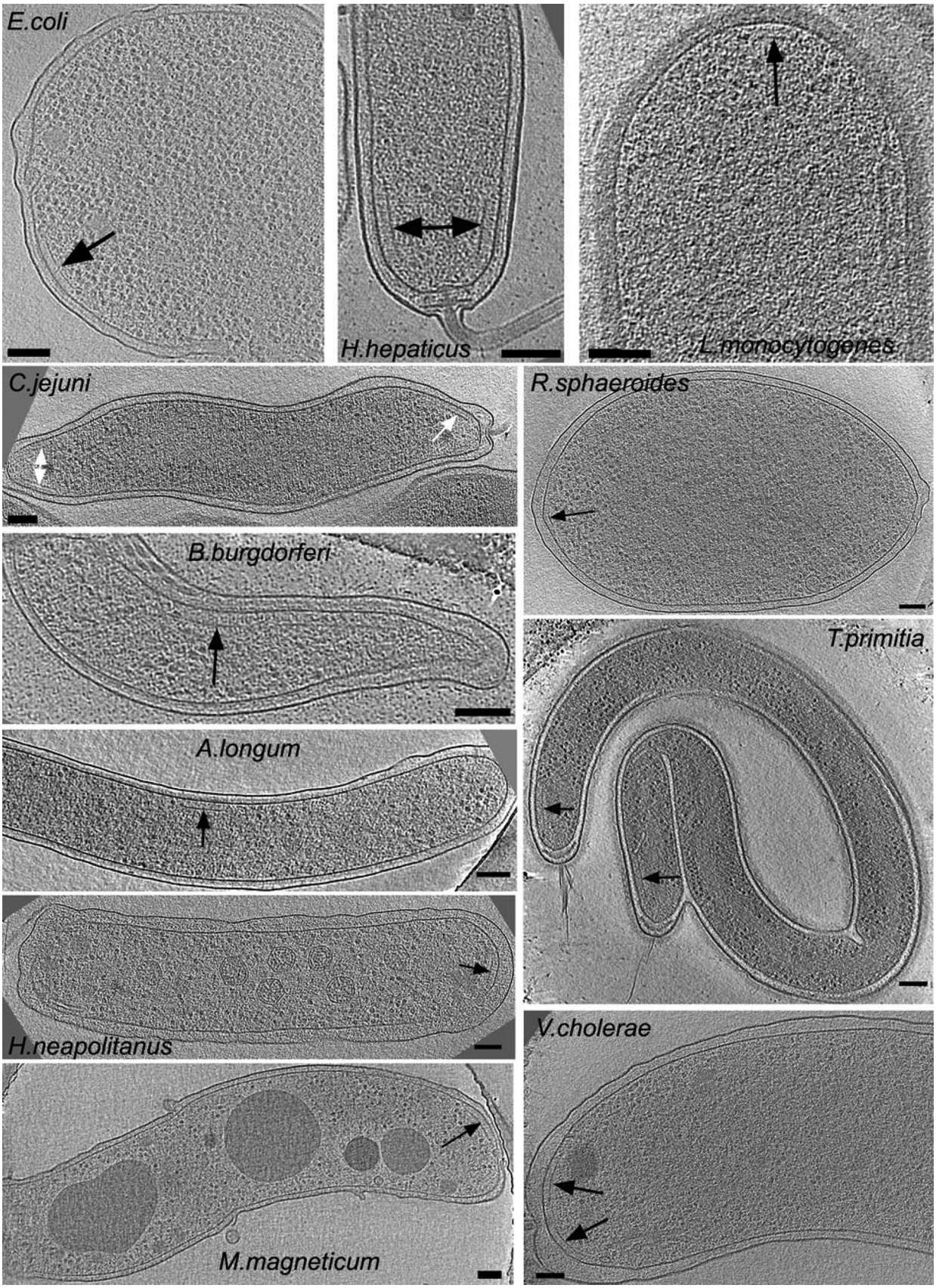

Fig. 2. Chemoreceptor arrays in diverse bacteria. Tomographic slices through cells of 11 different species illuminating the varied location but consistent appearance of the arrays. (*T. maritima* and *C. crescentus* are not shown, because they are available in Fig. 1 and ref. 21, respectively.) (Scale bars: 100 nm.)

cytoplasmic MCP arrays have been reported in *R. sphaeroides* (23–25), none were observed here.

Receptor Lengths. Despite the similarity of the arrays, the distance between the base plate and the inner membrane varied among species (Table 1). Measured values ranged from 21 nm in *R. sphaeroides* to 31 nm in *C. crescentus*, but were constant within each species. Because distinct periplasmic densities were observed above the arrays in nearly all of the cells, and only topology type I MCPs have large periplasmic domains, we infer that at least the majority of the MCPs composing these arrays were of topology type I. In 7 of the organisms imaged (*E. coli*, *V. cholerae*, *Halothiobacillus neapolitanus*, *A. longum*, *L. monocytogenes*, *R. sphaeroides*, and *T. maritima*), all of the topology type I MCPs in their respective genomes belong to a single (but different for each organism) signaling domain class (Table 1). When the observed distance between the inner membrane and base plate was plotted against the number of relevant residues (counted from the middle of TM2 to the conserved glycine at the tip of the hairpin) in the corresponding receptor sequences, there was a strong correlation with a slope of 0.142 nm per residue (Fig. 3*A*). Because all the MCPs shown in Fig. 3*A* contain a single HAMP domain, and its size is constant (26, 27), its presence should not affect the slope. The remarkable match of the observed slope with the rise per residue seen in the coiled coil crystal structure of a *T. maritima* receptor's signaling domain (0.145 nm/residue) (20) therefore strongly supports the sequence-based prediction (3) that the methylation, flexible bundle, and signaling sub-domains of all receptors are coiled coils in vivo.

The genomes of the other 6 organisms imaged (*C. jejuni*, *H. hepaticus*, *B. burgdorferi*, *T. primitia*, *M. magneticum*, and *C. crescentus*) each contain topology type I MCPs belonging to 2 different signaling domain classes, and some of their MCPs possess linkers and/or an additional HAMP domain (Fig. S1 *B* and *C*). It was therefore unclear which MCPs were forming the arrays in the imaged cells. When the observed receptor lengths were simply plotted against the total number of relevant residues in the various topology type I receptors present; however, in all but one of these organisms, only one of the 2 signaling domain classes matched the trend line (Fig. 3*B*). In the cases of *B. burgdorferi* and *T. primitia*, for instance, the class 48H MCPs matched the trend line, but the class 34H (*B. burgdorferi*) and unclassified (*T. primitia*) receptors did not. In the cases of *C. jejuni* and *H. hepaticus*, receptors of the 40H class matched the trend line, but those of class 28H, which contain long (≈95 residue) extra undefined regions between their HAMP and signaling domains (Fig. S1*C*), did not. In the case of *M. magneticum*, its class 38H receptors, which contain extra linkers (of ≈30 residues), fit the trend line, but its class 40H receptors did not. Finally, in the exceptional case of *C. crescentus*, both its class 36H and 38H receptors contain extra linkers, but neither matched the trend line well. However, close inspection of the sequences revealed that the class 36H receptors also contain a second HAMP domain. Because a HAMP domain is expected to be approximately 4 nm shorter than a (presumably) α-helical linker of the same number of residues (26), if this deficit is taken into account, the observed length of the class 36H receptors also matches the trend line well. Our interpretations are therefore that (*i*) in the single growth condition used for each particular species, the arrays were composed of receptors from a single predominant signaling class that could be identified by the observed distance between the inner membrane and base plate; (*ii*) the methylation, flexible bundle, and signaling sub-domains present in all 13 organisms are in fact coiled coils; and (*iii*) the linkers in the receptors imaged are α-helical in vivo. Assuming this is correct, our data contained images of 5 major signaling domain classes (44H, 40H, 38H, 36H, and 34H) and one minor signaling domain class (48H).

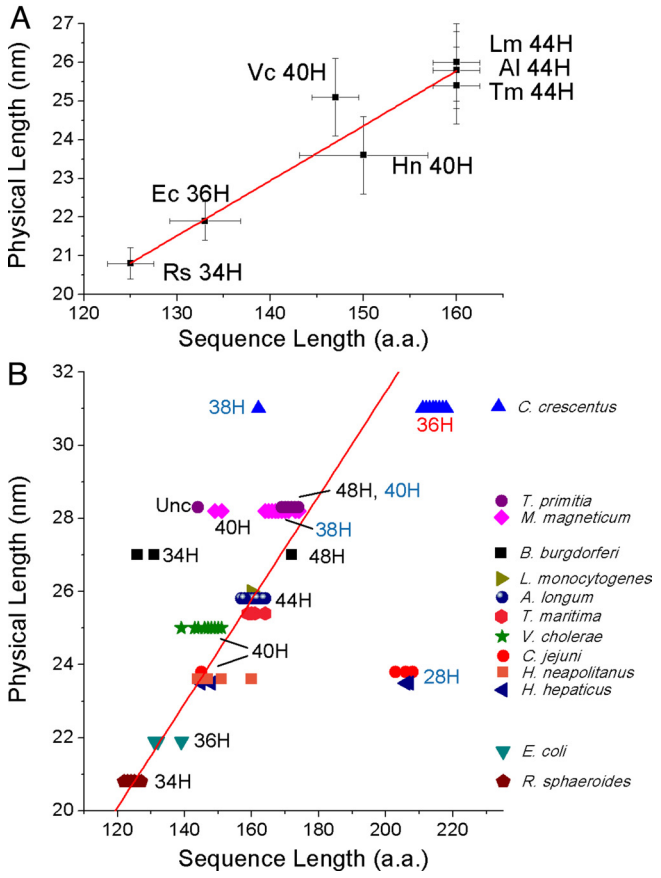

Fig. 3. Correlation between observed physical length and predicted sequence length. (*A*) Organisms possessing a single class of topology type I receptors. Physical length and sequence length were measured as described in *Materials and Methods*. The sequence length is an average of all topology type I MCPs in the given genome. Vertical bars indicate SD of measurements from different cryo-tomograms and positions within the array, horizontal bars indicate the larger of the SD of the various MCP sequence lengths present in the genome or the estimated uncertainty in the position of the transmembrane region (≈5 residues, see *Materials and Methods*). The line is a least-squares fit whose slope confirms that the cytoplasmic domains of the receptors form extended coiled coils. *Al*, *A. longum*; *Ec*, *E. coli*; *Hn*, *H. neapolitanus*; *Lm*, *L. monocytogenes*; *Rs*, *R. sphaeroides*; *Tm*, *T. maritima*; and *Vc*, *V. cholera*. (*B*) All topology type I MCPs in all 13 organisms imaged. Each MCP sequence in each organism is represented by a symbol, color- and shape-coded by organism (*Right*). All the MCPs of a particular organism appear at the same height on the graph (the measured distance between the inner membrane and base plate layer), even though it is not known which were actually imaged. MCPs of particular signaling domain classes cluster closely (3), and are labeled with the color of the label itself (e.g., *34H*, *36H*) indicating whether the receptors of that class are typical (black), contain extra linkers (blue), or contain both extra linkers and a second HAMP domain (red; see Fig. S1*C*). The sequence lengths of typical receptors (i.e., those without extra linkers and HAMP domains) are seen to progress steadily with class number across the graph from left to right. Receptors with additional linkers or a second HAMP domain (blue and red labels) appear further to the right than expected because of their extra residues. The Unc label represents an MCP that does not correspond to a known length class, but was given a sequence length measurement as described in *Materials and Methods*. The graph shows that within the organisms that possess 2 classes of receptors (*C. jejuni*, *H. hepaticus*, *B. burgdorferi*, *T. primitia*, *M. magneticum*, and *C. crescentus*), only one class matches the trend line found in *A*, suggesting that it was the receptor class forming the arrays.

Lattice Arrangement. Eleven of the species imaged here presented clear "top" views (i.e., slices parallel to the cytoplasmic membrane) of the arrays (those of *L. monocytogenes* and *B. burgdorferi* were inaccessible; see Fig. 4). Surprisingly, they all revealed

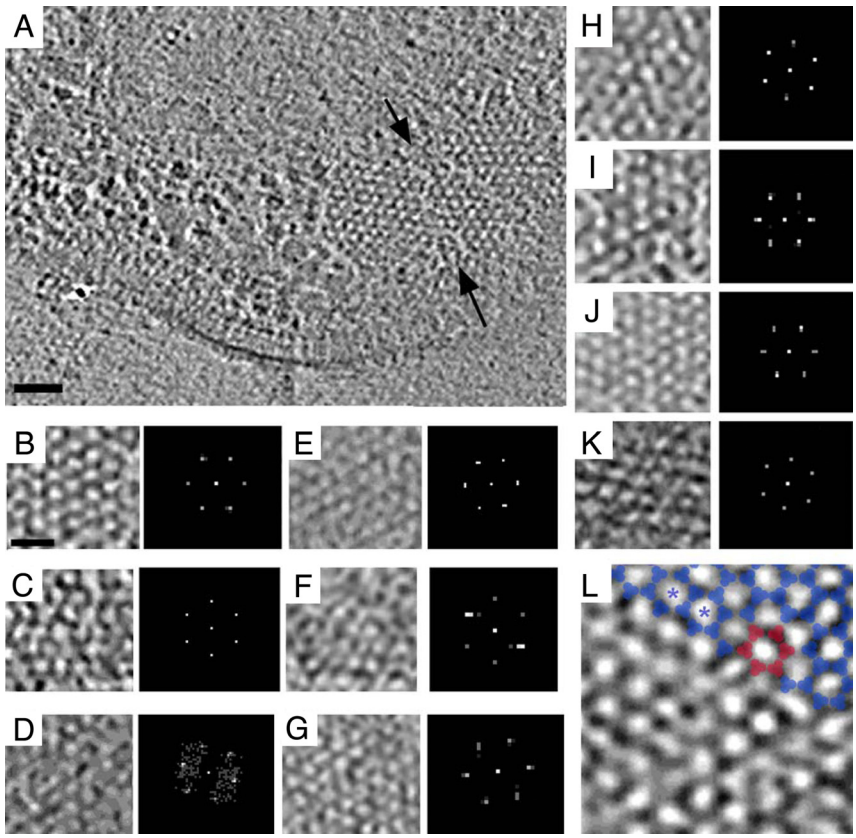

Fig. 4. Universally conserved 12-nm hexagonal arrangement of receptor. (*A*) ''Top'' view of a chemoreceptor array (black arrows) in *T. maritima* (signaling domain class 44H). (Scale bar: 50 nm.) (*B–K*) Top views (*Left*) and power spectra (*Right*) of receptor arrays all reveal the same ≈12-nm hexagonal lattice. *B*, *T. maritima*; *C*, *A. longum*; *D*, *C. jejuni*; *E*, *H. hepaticus*; *F*, *M. magneticum*; *G*, *H. neapolitanus*; *H*, *R. sphaeroides*; *I*, *E. coli*; *J*, *V. cholerae*; *K*, *T. primitia*. (Scale bars: 25 nm; power spectra enlarged.) (*L*) Trimer of dimers (blue) fit into the vertices of the hexagonal lattice in a chemoreceptor array (*V. cholerae*). Six trimers of dimers (red) enclose one hexagon. The spacing from the center of one hexagon to the center of an adjacent one is consistently 12 nm (blue asterisks).

the same approximate 12-nm honeycomb-like hexagonal arrangement immediately above the base layer as observed previously in *C. crescentus*. We conclude that, throughout the entire wide range of species and receptor classes imaged here [including WT *E. coli* and *T. maritima,* for which MCP crystal structures and alternative models exist, as well as organisms from 6 diverse taxonomic groups that span the bacterial kingdom (Fig. S2 and *SI Appendix*)], trimers of receptor dimers pack at the vertices of a 12-nm hexagonal lattice. In all the arrays we observed, the honeycomb-like lattice was clearest just above the base plate but deteriorated as it rose toward the inner membrane. These observations support the notion that the major architectural contacts occur near the signaling sub-domain of chemoreceptors (4). Although the basic arrangement of all of the arrays was clearly hexagonal, none of the arrays were perfectly regular, supporting the idea that the degree of local order could reflect activation and/or regulation (22). The size of the arrays, and thus the estimated number of receptors, varied by an order of magnitude (from ≈1,200 in *M. magneticum* to ≈14,400 in *C. jejuni*; Table 1), without obvious correlation to the cell size or bacterial taxonomy.

Conclusion

Tightly coupled, communicating chemoreceptor arrays are thought to enable the main features of the signaling mechanism: heightened sensitivity (28), signal gain (29), cooperativity (30, 31), and adaptation (32, 33). The universal hexagonal architecture and secondary structure of chemoreceptor arrays we observed in diverse bacterial species therefore implies that the trimer-of-dimers arrangement and the underlying signaling mechanism are preserved over long evolutionary distances (Fig. S2). The main features of the signaling mechanism that are being revealed in *E. coli* are therefore likely to be applicable to other bacterial species. This is important because, although chemotaxis is critical to pathogenic (34) and symbiotic (35) interactions of bacteria with higher organisms, the molecular details of this system can at present be studied in only a few model organisms.

Materials and Methods

Strains, Sample Preparation, EM Data Collection, and Image Processing. Bacterial strains [*C. crescentus* CB15N, *E. coli* RP437 and MG1655, *T. maritima* MSB8/DSM 3109, *V. cholerae* TRH7000, *M. magneticum* sp. AMB-1, *H. hepaticus* ATCC 51449, *C. jejuni* ATCC 29428, *R. sphaeroides* NCIB 8253, *B. burgdorferi* B31 cells ATCC 35210, *L. monocytogenes* strain 10403S (serotype 1/2a), *A. longum* APO-1 DSM 6540, *T. primitia* strain ZAS-2, *H. neapolitanus* C2 ATCC 23641] were grown in standard media. To flatten the thickest cell types slightly, *E. coli* cells were incubated with 462 IU/mL penicillin G for 60 min at 30 °C (36) and *T. maritima* cells were treated with 1 mg/mL polymyxin B for 10 h on ice. Cultures were plunge-frozen across EM grids as described (37). Standard EM tilt series were collected on 300 kV electron cryo-microscopes and 3D reconstructions were calculated as described (38, 39). The hexagonal arrangement of the arrays was clearly evident in both the raw tomographic slices and their power spectra. *SI Text* contains further details.

MCP Sequences and Classification. MCP sequences from the complete genomes (*E. coli*, *C. crescentus*, *T. maritima*, *V. cholerae*, *M. magneticum*, *H. hepaticus*, *C. jejuni*, *R. sphaeroides*, *B. burgdorferi*, *L. monocytogenes*) were downloaded from the MIST database (40). For the draft genomes (*A. longum*, *T. primitia*, and *H. neapolitanus),* contigs were subjected to the GeneMark gene finding program (41) to obtain the translated sequences. MCPs were then identified

MICROBIOLOGY

in translated proteins using the MCPsignal domain model [Pfam database (42) accession number PF00015] and the HMMER software package (43). The final set contained 223 MCPs from 13 genomes (Table 1). MCPs were assigned to signaling classes and membrane topology types as previously described (3, 44). Sequences that did not match any established signaling class were left unclassified (''unc'' in Table 1).

Physical and Sequence Length Measurements. Because of the well understood point-spread function in ECT (including a final low-pass filter), the edges of objects appear less sharp in tomograms than they really are. The exact positions of the top and bottom of the inner membrane or CheAW base plate are therefore difficult to ascertain. However, the location of their midplanes are highly reliable, as the point-spread function only smooths (and does not shift) peaks. The distance between the peaks (i.e., midplanes) of the inner membrane and CheAW base plate was therefore used as an estimate of the physical length of the cytoplasmic portion of the MCPs. Likewise, the center of transmembrane regions can be more reliably predicted from sequence than the edges, and neither is exact because transmembrane helices likely drift up and down a few residues within the fluid bilayer. The sequence length of the ''cytoplasmic'' domains was therefore taken to be the number of amino acids from the middle of TM2 to the conserved glycine at the tip of the hairpin (Gly-390 in the Tsr protein of *E. coli*; Fig. S1*A*). Although it is not yet known exactly where the tip of the hairpin is with respect to the midplane of the CheAW base plate, because whatever discrepancy that might exist is likely to be the same for all the receptors, it should not affect the slope of the correlation between physical and sequence lengths across different receptor classes.

ACKNOWLEDGMENTS. The authors wish to thank Eric Matson, Reinhard Rachel, Kevin Bruhn, Gordon Cannon, Alan Barbour, Sarkis Mazmanian, Jeanette Beatty, Maria Sandkvist, Dianne Newman, and John S. Parkinson for bacterial strains; Howard Berg for the penicillin treatment protocol for *E. coli*; Jane H. Ding for computational support; Juergen Plitzko, Alasdair McDowall and Jian Shi for EM support; and Roger Alexander, Luke Ulrich, and Bhanu Rekapalli for assistance and helpful suggestions. The authors also thank Professor Wolfgang Baumeister (Max Planck Institute for Biochemistry, Martinsried, Germany) for the permission to include the data from *T. maritima* (which was collected in his laboratory and under his supervision) in this study. This work was supported in part by National Institutes of Health Grants R01 AI067548 and P50 GM082545 (to G.J.J.) and R01 GM72285 (to I.B.Z.), as well as the Howard Hughes Medical Institute, the Beckman Institute at Caltech, and gifts to Caltech from the Gordon and Betty Moore Foundation and Agouron Institute.

1. Wadhams GH, Armitage JP (2004) Making sense of it all: bacterial chemotaxis. *Nat Rev Mol Cell Biol* 5:1024–1037.
2. Zhulin IB (2001) The superfamily of chemotaxis transducers: from physiology to genomics and back. *Adv Microb Physiol* 45:157–198.
3. Alexander RP, Zhulin IB (2007) Evolutionary genomics reveals conserved structural determinants of signaling and adaptation in microbial chemoreceptors. *Proc Natl Acad Sci USA* 104:2885–2890.
4. Hazelbauer GL, Falke JJ, Parkinson JS (2008) Bacterial chemoreceptors: high-performance signaling in networked arrays. *Trends Biochem Sci* 33:9–19.
5. Boukhvalova MS, Dahlquist FW, Stewart RC (2002) CheW binding interactions with CheA and Tar: importance for chemotaxis signaling in *E. coli*. *J Biol Chem* 277:22251–22259.
6. Bray D, Levin MD, Morton-Firth CJ (1998) Receptor clustering as a cellular mechanism to control sensitivity. *Nature* 393:85–88.
7. Gestwicki JE, Kiessling LL (2002) Inter-receptor communication through arrays of bacterial chemoreceptors. *Nature* 415:81–84.
8. Lybarger SR, Maddock J (2001) Polarity in action: asymmetric protein localization in bacteria. *J Bacteriol* 183:3261–3267.
9. Maddock JR, Shapiro L (1993) Polar location of the chemoreceptor complex in the *Escherichia coli* cell. *Science* 259:1717–1723.
10. Kim KK, Yokota H, Kim SH (1999) Four-helical-bundle structure of the cytoplasmic domain of a serine chemotaxis receptor. *Nature* 400:787–792.
11. Boldog T, Grimme S, Mingshan L, Sligar SG, Hazelbauer GL (2006) Nanodiscs separate chemoreceptor oligomeric states and reveal their signaling properties. *Proc Natl Acad Sci USA* 103:11509–11514.
12. Studdert CA, Parkinson JS (2007) In vivo crosslinking methods for analyzing the assembly and architecture of chemoreceptor arrays. *Methods Enzymol* 423:414–431.
13. Shimizu TS, et al. (2000) Molecular model of a lattice of signalling proteins involved in bacterial chemotaxis. *Nat Cell Biol* 2:792–796.
14. Khursigara CM, Wu X, Zhang P, Lefman J, Subramaniam S (2008) Role of HAMP domains in chemotaxis signaling by bacterial chemoreceptors. *Proc Natl Acad Sci USA* 105:16555–16560.
15. Lefman J, et al. (2004) Three-dimensional electron microscopic imaging of membrane invaginations in *Escherichia coli* overproducing the chemotaxis receptor Tsr. *J Bacteriol* 186:5052–5061.
16. Weis RM, et al. (2003) Electron microscopic analysis of membrane assemblies formed by the bacterial chemotaxis receptor Tsr. *J Bacteriol* 185:3636–3643.
17. Zhang P, et al. (2004) Direct visualization of receptor arrays in frozen-hydrated sections and plunge-frozen specimens of *E. coli* engineered to overproduce the chemotaxis receptor Tsr. *J Microsc* 216:76–83.
18. Wolanin PM, Baker MD, Thomas DR, DeRosier DJ, Stock AM (2006) Self-assembly of receptor/signaling complexes in bacterial chemotaxis. *Proc Natl Acad Sci USA* 103:14313–14318.
19. Zhang P, Khursigara CM, Hartnell LM, Subramaniam S (2007) Direct visualization of *Escherichia coli* chemotaxis receptor arrays using cryo-electron microscopy. *Proc Natl Acad Sci USA* 104:3777–3781.
20. Park SY, et al. (2006) Reconstruction of the chemotaxis receptor-kinase assembly. *Nat Struct Mol Biol* 13:400–407.
21. Briegel A, et al. (2008) Location and architecture of the *Caulobacter crescentus* chemoreceptor array. *Mol Microbiol* 69:30–41.
22. Khursigara CM, Wu X, Subramaniam S (2008) Chemoreceptors in *Caulobacter crescentus*: trimers of receptor dimers in a partially ordered hexagonally packed array. *J Bacteriol* 190:6805–6810.
23. Porter SL, Wadhams GH, Armitage JP (2008) *Rhodobacter sphaeroides*: complexity in chemotactic signaling. *Trends Microbiol* 16:251–260.
24. Wadhams GH, et al. (2002) TlpC, a novel chemotaxis protein in *Rhodobacter sphaeroides*, localizes to a discrete region in the cytoplasm. *Mol Microbiol* 46:1211–1221.
25. Wadhams GH, Warren AV, Martin AC, Armitage JP (2003) Targeting of two signal transduction pathways to different regions of the bacterial cell. *Mol Microbiol* 50:763–770.
26. Hulko M, et al. (2006) The HAMP domain structure implies helix rotation in transmembrane signaling. *Cell* 126:929–940.
27. Aravind L, Ponting CP (1999) The cytoplasmic helical linker domain of receptor histidine kinase and methyl-accepting proteins is common to many prokaryotic signalling proteins. *FEBS Microbiol Lett* 176:111–116.
28. Duke TAJ, Bray D (1999) Heightened sensitivity of a lattice of membrane receptors. *Proc Natl Acad Sci USA* 96:10104–10108.
29. Sourjik V, Berg H (2002) Receptor sensitivity in bacterial chemotaxis. *Proc Natl Acad Sci USA* 99:123–127.
30. Li G, Weis RM (2000) Covalent modification regulates ligand binding to receptor complexes in the chemosensory system of *Escherichia coli*. *Cell* 100:357–365.
31. Sourjik V, Berg HC (2004) Functional interactions between receptors in bacterial chemotaxis. *Nature* 428:437–441.
32. Endres RG, Wingreen NS (2006) Precise adaptation in bacterial chemotaxis through ''assistance neighborhoods.'' *Proc Natl Acad Sci USA* 103:13040–13044.
33. Li M, Hazelbauer GL (2005) Adaptational assistance in clusters of bacterial chemoreceptors. *Mol Microbiol* 56:1617–1626.
34. Butler SM, Camilli A (2004) Both chemotaxis and net motility greatly influence the infectivity of *Vibrio cholerae*. *Proc Natl Acad Sci USA* 101:5018–5023.
35. Miller LD, Yost CK, Hynes MF, Alexandre G (2007) The major chemotaxis gene cluster of *Rhizobium leguminosarum* bv. viciae is essential for competitive nodulation. *Mol Microbiol* 63:348–362.
36. Eisenbach M, Adler J (1981) Bacterial cell envelopes with functional flagella. *J Biol Chem* 256:8807–8814.
37. Iancu CV, et al. (2007) Electron cryotomography sample preparation using the Vitrobot. *Nat Protoc* 1:2813–2819.
38. Mastronarde DA (1997) Dual-axis tomography: an approach with alignment methods that preserve resolution. *J Struct Biol* 120:343–352.
39. Hegerl R (1996) The EM program package: a platform for image processing in biological electron microscopy. *J Struct Biol* 116:30–34.
40. Ulrich LE, Zhulin IB (2007) MiST: a microbial signal transduction database. *Nucleic Acids Res* 35:D386–D390.
41. Besemer J, Borodovsky M (2005) GeneMark: web software for gene finding in prokaryotes, eukaryotes and viruses. *Nucleic Acids Res* 33:W451–W454.
42. Finn RD, et al. (2008). The Pfam protein families database. *Nucleic Acids Res* 36:D281–D2288.
43. Eddy SR (1998) Profile hidden Markov models. *Bioinformatics* 14:755–763.
44. Wuichet K, Alexander RP, Zhulin IB (2007) Comparative genomic and protein sequence analyses of a complex system controlling bacterial chemotaxis. *Methods Enzymol* 422:1–31.